Direct observations of the full Dungey convection cycle in the polar ionosphere for southward interplanetary magnetic field conditions

Article

Published Version

the End User Agreement.

www.reading.ac.uk/centaur

CentAUR

Central Archive at the University of Reading

Reading's research outputs online

RESEARCH ARTICLE

Key Points:
- Direct observations of the full Dungey cycle by tracking polar cap patches
- Formation and evolution of patches modulated by dayside and nightside reconnections
- The full circulation time was about 3 h

Supporting Information:
- Text S1
- Movie S1

Correspondence to:
Q.-H. Zhang,
zhangqinghe@sdu.edu.cn

Direct observations of the full Dungey convection cycle in the polar ionosphere for southward interplanetary magnetic field conditions

Q.-H. Zhang[1], M. Lockwood[2], J. C. Foster[3], S.-R. Zhang[3], B.-C. Zhang[4], I. W. McCrea[5], J. Moen[6], M. Lester[7], and J. M. Ruohoniemi[8]

[1]Shandong Provincial Key Laboratory of Optical Astronomy and Solar-Terrestrial Environment, Institute of Space Sciences, Shandong University, Weihai, China, [2]Department of Meteorology, University of Reading, Berkshire, UK, [3]MIT Haystack Observatory, Westford, Massachusetts, USA, [4]SOA Key Laboratory for Polar Science, Polar Research Institute of China, Shanghai, China, [5]Space Sciences Division, SSTD, Rutherford Appleton Laboratory, Didcot, UK, [6]Department of Physics, University of Oslo, Oslo, Norway, [7]Department of Physics and Astronomy, University of Leicester, Leicester, UK, [8]Bradley Department of Electrical and Computer Engineering, Virginia Tech, Blacksburg, Virginia, USA

Abstract Tracking the formation and full evolution of polar cap ionization patches in the polar ionosphere, we directly observe the full Dungey convection cycle for southward interplanetary magnetic field (IMF) conditions. This enables us to study how the Dungey cycle influences the patches' evolution. The patches were initially segmented from the dayside storm enhanced density plume at the equatorward edge of the cusp, by the expansion and contraction of the polar cap boundary due to pulsed dayside magnetopause reconnection, as indicated by in situ Time History of Events and Macroscale Interactions during Substorms (THEMIS) observations. Convection led to the patches entering the polar cap and being transported antisunward, while being continuously monitored by the globally distributed arrays of GPS receivers and Super Dual Auroral Radar Network radars. Changes in convection over time resulted in the patches following a range of trajectories, each of which differed somewhat from the classical twin-cell convection streamlines. Pulsed nightside reconnection, occurring as part of the magnetospheric substorm cycle, modulated the exit of the patches from the polar cap, as confirmed by coordinated observations of the magnetometer at Tromsø and European Incoherent Scatter Tromsø UHF radar. After exiting the polar cap, the patches broke up into a number of plasma blobs and returned sunward in the auroral return flow of the dawn and/or dusk convection cell. The full circulation time was about 3 h.

1. Introduction

The Dungey convection cycle is a fundamental space physics process, resulting in energy and momentum transfer from the solar wind to the magnetosphere and circulation in the coupled magnetosphere-ionosphere system. This convection cycle is seen in the flow of ionospheric plasma antisunward over the polar cap and the sunward return flow immediately outside the polar cap in the auroral ovals [*Dungey*, 1961]. It has two causes: reconnection in the magnetopause, which generates "open" magnetic flux that is connected to the interplanetary magnetic field embedded in the solar wind flow and reconnection in the cross-tail current sheet which recloses the magnetic flux, enabling it to migrate sunward, back to the dayside, and so complete the cycle. Steady state, in which these two reconnection voltages are equal, is rarely achieved and the normal behavior involves the substorm cycle, in which the magnetopause reconnection voltage dominates in the initial "growth" phase, but the tail reconnection voltage dominates in the later "expansion" and "recovery" phases [*McPherron et al.*, 1973]. The instantaneous ionospheric flow patterns for the Dungey cycle during substorms are given by the expanding-contracting polar cap (ECPC) model [*Cowley and Lockwood*, 1992; *Siscoe and Huang*, 1985], which includes two basic time-dependent components to drive the flow: one is the magnetopause coupling process (dayside reconnection) [e.g., *Dunlop et al.*, 2011] and the other is the magnetotail reconnection process [e.g., *Hones and Schindler*, 1979]. Over the past 50 years, considerable effort has been expended to elucidate the nature of these flows and the energy transport rate in the full Dungey cycle. For instance, *Milan et al.* [2007] surveyed the dayside and nightside reconnection rates for the magnetic flux transport in the Dungey cycle by using a large data set (with observations including satellite in situ particle data, global auroral observations, and ground-based

radar measurements). It is impossible, however, to track a single reconnected field line (and the plasma frozen on to it, collectively referred to as a flux tube) through the magnetosphere for a full Dungey cycle, simply because of the huge extent of the magnetosphere. The ionosphere offers a unique opportunity to image the cyclic motion of flux tubes. A clear distinction must be made, however, between the loci of the ionospheric feet of flux tubes and the streamlines (equipotentials) of the pattern of ionospheric convection. Only in the steady state situation are these the same and although the convection pattern gives the direction and speed of travel of a flux tube at any one instant, in the general, nonsteady case, its locus will depend on the history of changes of the convection pattern [*Lockwood*, 1993]. Thus, convection patterns from radars and magnetometer networks at any one time do not tell us about the trajectories of flux tubes in the general, nonsteady case. This concept is important for understanding the evolution of high-latitude *F* region ionospheric plasma (and of plasma structures like patches), which depends on the locus of the flux tube [*Lockwood*, 1993].

Polar cap patches are defined as islands of high-density ionospheric plasma poleward of the auroral oval, surrounded by plasma of half the density or less [*Crowley*, 1996]. It was recognized at an early stage that midlatitude ionospheric plasma, produced by solar EUV, provided a viable reservoir of source plasma for both discrete polar cap patches or for a continuous tongue of ionization (TOI), with the plasma being drawn by convection into the polar cap [*Knudsen*, 1974; *Foster and Doupnik*, 1984; *Foster et al.*, 2005]. In addition, on entry into the polar cap the flux tube is subjected to the cleft-cusp-mantle magnetosheath plasma precipitation sequence [*Lockwood*, 1997], which enhances and heats the ionospheric plasma [*Rodger et al.*, 1994].

Previous works [*Lockwood and Carlson*, 1992; *Lockwood et al.*, 2005; *Q.-H. Zhang et al.*, 2011, 2013a] have demonstrated that observations of polar cap patches can be used to infer the variability of magnetopause reconnection, which was confirmed by Time History of Events and Macroscale Interactions during Substorms (THEMIS) in situ observations [*Walsh et al.*, 2014]. *Zhang et al.* [2013b] also reported that the exit of the patches from the polar cap is modulated by pulsed nightside reconnection, occurring as part of the magnetospheric substorm cycle, consistent with observations of TOI/patch cold plasma density at 5.5 *Re* altitude at midnight (with coincident GPS total electron content (TEC) mapping) at the position of a substorm depolarization [*Foster et al.*, 2014]. Hence, the movement of polar cap patches can be used to track the loci of flux tubes as they evolve around the full Dungey convection cycle [*Zhang et al.*, 2013b; *Oksavik et al.*, 2010].

In this paper, we present continuous monitoring of flux tubes undergoing the Dungey cycle, using both plasma density and flow over a large fraction of the northern hemisphere convection zone during a full convection cycle (5 h, with time resolution of 5 min) by combining observations of the total electron content (TEC) from the large and dense array of GPS receivers [*Coster et al.*, 2003] with the large-scale coverage of the flows provided by the Super Dual Auroral Radar Network (SuperDARN) radars using the "Map Potential" technique [*Ruohoniemi and Baker*, 1998; *Chisham et al.*, 2007; *Thomas et al.*, 2013], together with measurements from the magnetometer at Tromsø and the European Incoherent Scatter (EISCAT) Tromsø UHF radar.

2. Observations

2.1. Upstream Solar Wind and Interplanetary Magnetic Field Conditions

On 17 January 2013, a coronal mass ejection impacted the magnetopause, giving an enhancement of solar wind dynamic pressure, P_{Dyn} and resulting in a small geomagnetic storm (*Dst*, minimum of -53 nT) [*Walsh et al.*, 2014]. A reverse shock (sudden decrease in P_{Dyn} mainly due to a sudden decrease in solar wind number density) impacted the magnetosphere at about 15:30 UT. In Figure 1, we present an overview of the solar wind and interplanetary magnetic field (IMF) conditions from the OMNI-2 data set (based on the measurements from the Wind and ACE satellites) [*King and Papitashvili*, 2005] during the period 14:00–24:00 UT. Parameters shown are (a) the GSM IMF components, (b) the IMF clock angle (CA), (c) the solar wind plasma number density (N_{SW}), (d) the solar wind speed (*V*), and (e) the solar wind dynamic pressure (P_{dyn}). The data have been lagged by 5 min to allow for the propagation delay from the nose of bow shock to the dayside magnetopause. Right at and after the reverse shock, the IMF B_x and B_y components changed their polarity three times and remained weakly sunward and strongly dawnward after about 17:06 UT, while the IMF B_z stayed strongly negative, except for a short positive excursion from
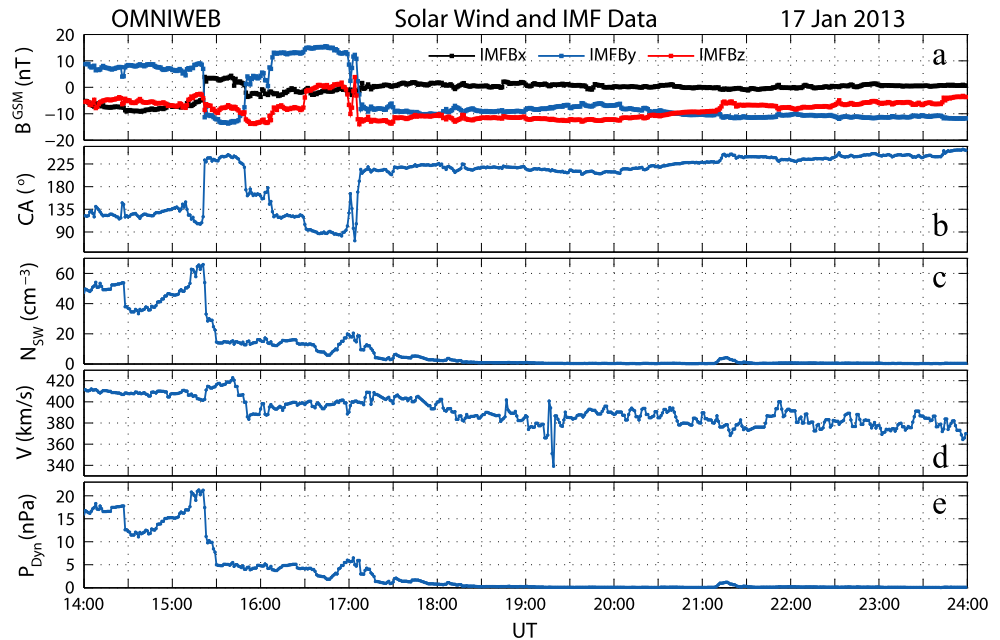
Figure 1. An overview of the solar wind and IMF conditions from the OMNI-2 data set (based on measurements from the Wind and ACE satellites). Parameters shown are (a) the GSM IMF components, (b) the IMF clock angle (CA), (c) the solar wind plasma number density (N_{SW}), (d) the solar wind speed (V), and (e) the solar wind dynamic pressure (P_{dyn}). The data have been lagged by 5 min to allow for propagation from the nose of bow shock to the magnetopause.

16:31 to 17:00 UT (see Figure 1a). Hence, the IMF clock angle varied from 204° to 250° while the IMF magnitude was large (>10 nT) for an extended period after 17:06 UT (see Figure 1b), favoring a high magnetopause reconnection rate. The solar wind density varied between about 34 and 64 cm^{-3} before the reverse shock and decreased to about 2 cm^{-3} after 17:18 UT (see Figure 1c), while the solar wind velocity varied between 360 and 420 km/s (see Figure 1d), resulting in a prevailing solar wind dynamic pressure in the range 11–21 nPa before the reverse shock and in the range 0–2 nPa after 17:18 UT (see Figure 1f).

2.2. GPS TEC Data and SuperDARN Convection Maps

Figure 2 shows the formation and evolution of patches, as revealed by mapping of the GPS TEC and the SuperDARN convection patterns. The patches are characterized by local enhancements in TEC and highlighted by the magenta circles or ellipses with numbers from P1 to P5. Note the change in scale used in Figure 2 to better show the evolution of the patches. The different colors represent different TEC values as shown by the color bars, where Figures 2a–2d use the upper color bar with a range of 0–20 TEC unit (TECU; 1 TECU $= 10^{16}$ el m^{-2}) and Figures 2e–2i use the lower color bar with a range of 0–15 TECU. The TEC unit is the standard unit for expressing total electron content, corresponding to the total number of electrons contained in a column of cross-sectional area 1 m^2, extending upward from the Earth's surface through the ionosphere. One TECU is defined as 1×10^{16} el/m^2. The dashed black with red circle in each panel shows the Heppner-Maynard Boundary (HMB) [*Heppner and Maynard*, 1987], which represents the latitudinal extent of the ionospheric convection pattern inferred from the SuperDARN radar observations [*Shepherd and Ruohoniemi*, 2000] and whose equatorward motion indicates expansion to lower latitudes. The expansion or contraction of the convection pattern as a whole is linked to, but not the same as, the expansion or contraction of the polar cap [e.g., *Imber et al.*, 2013]. The dotted line across each panel is the day-night terminator at 100 km altitude. Figure 2a shows a typical two-cell convection pattern as observed by SuperDARN radars using the Map Potential technique, with large values of GPS TEC in the dayside lower latitude region due to the solar EUV ionization, but generally small TEC poleward of the HMB and in the lower latitude region of the nightside sector. The region of high-density sunlit plasma is inclined toward the duskside, with a cavity of lower-density plasma around 60° magnetic latitude and before 10:00 magnetic local time (MLT), due to the combined effect of the Earth's rotation and polar ionospheric convection. This interval corresponded to the growth phase of a small substorm (as revealed by the AE
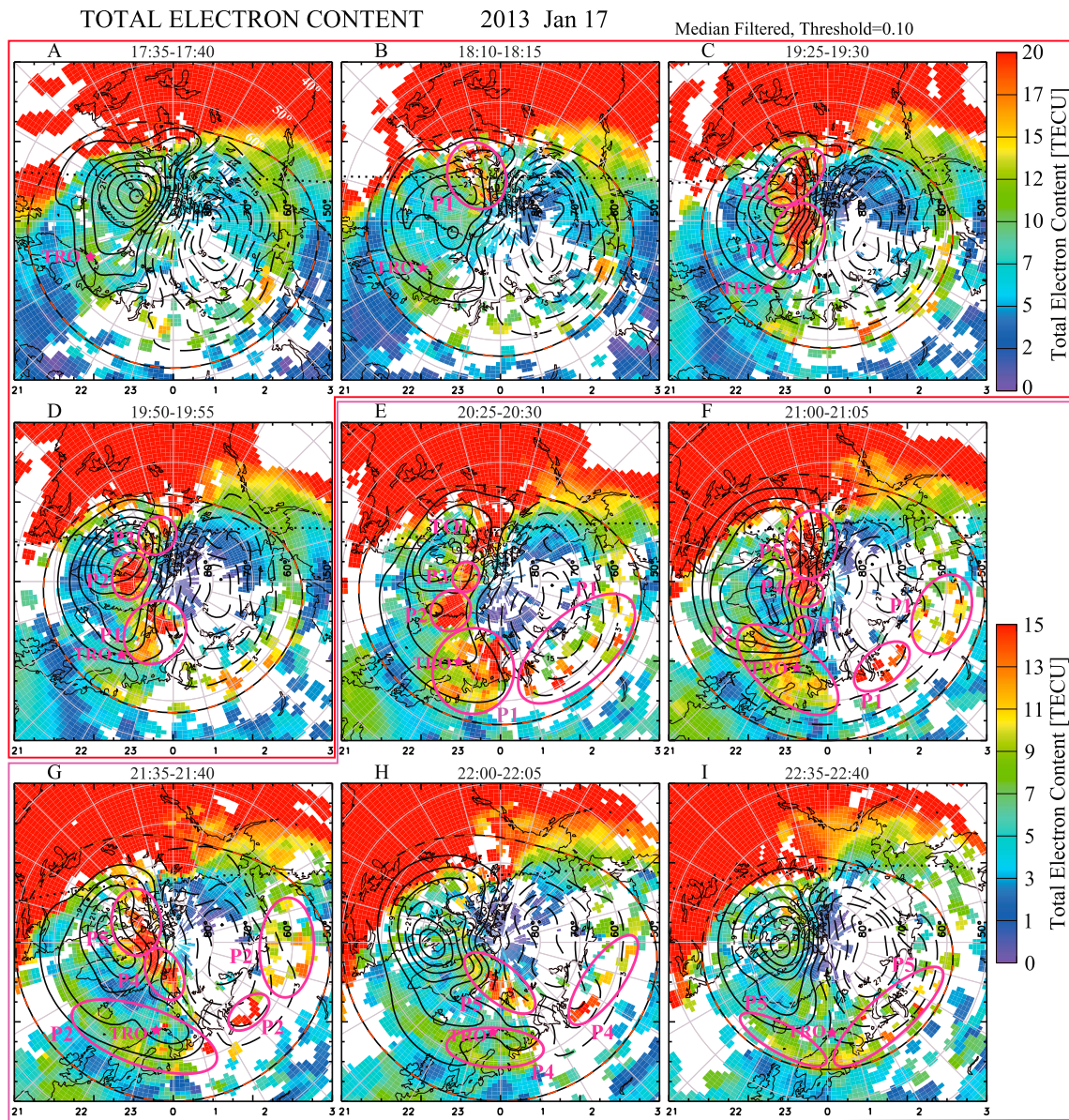
Figure 2. Selected examples from a full series of 2-D maps of median-filtered TEC and ionospheric convection on a geomagnetic latitude/MLT grid with noon at the top (Movie S1 in the supporting information). The dotted line across each panel is the day-night terminator at 100 km altitude. The magenta circles and ellipses with numbers P1–P5 highlight the polar cap patches, the evolutions of which are followed here. The mauve star with a TRO represents the location of Tromsø, where the EISCAT Tromsø UHF radar and Tromsø magnetometer are located (data from which are shown in Figure 4).

index, not shown here) and at such times the dayside polar cap boundary (PCB) should expand equatorward, as predicted by the ECPC model [*Cowley and Lockwood*, 1992; *Siscoe and Huang*, 1985] as do the Region 2 currents and hence the HMB [*Iijima and Potemra*, 1978; *Bythrow et al.*, 1984]. The polar cap expansion is caused by an increase in the global dayside reconnection rate, and the Region-2/HMB motion is a response to the growth of open flux and transpolar voltage [*Siscoe*, 1982]. The equatorward motion of the low-latitude edge of the convection pattern (the HMB) takes place rapidly, because the currents that shield lower latitudes from the polar electric field take time to establish [*Kelley et al.*, 1979]. Hence, transient enhancements in convection can lead to short-lived subauroral flows (collectively known as subauroral polarization streams [*Foster and Burke*, 2002]), which can reach deep into the plasmasphere and cause it to erode by convecting dusk-sector magnetospheric flux tubes (called detached plasma regions [*Chappell*, 1974]) toward the near-noon magnetopause, where the plasma is lost to the magnetosheath as the field
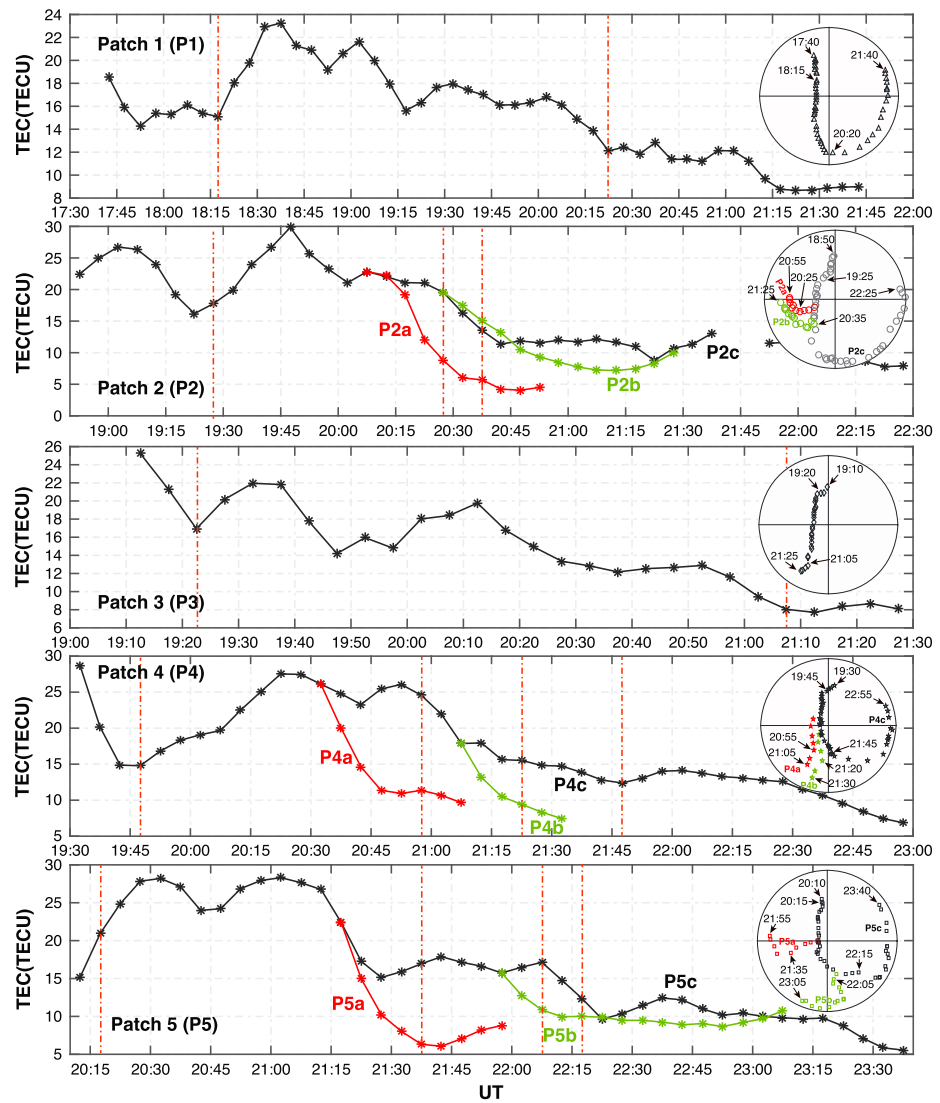
Figure 3. The time series evolution of the TEC and the trajectories of selected points at the leading edge of each patch.

line is opened by reconnection [*Goldstein et al.*, 2003]. The ionospheric signature of such a plasmasphere erosion event is seen as the storm enhanced density plume (SED) [*Foster et al.*, 2004], which transports EUV-enhanced plasma in the afternoon sector toward the cleft/cusp region and thence into the polar cap through the "convection throat." During the time period under investigation, in situ measurements at the dayside magnetopause made by the THEMIS spacecraft confirmed that active reconnection was occurring at the boundary [*Walsh et al.*, 2014], a necessary requirement for the above sequence of events. After this expansion, the polar cap boundary contracted poleward and the EUV-enhanced plasma that had become entrained in the convection pattern was transported toward the convection throat to form a plasma patch (patch P1 in Figure 2b). Such expansion and contraction of the PCB occurred repeatedly, due to pulsed reconnection at the dayside magnetopause, and helped to form a series of patches in the polar ionosphere (patches P1–P5), which moved poleward toward the nightside after formation, with a growth in their size around the cusp region (shown in Figures 2c–2h), which would be consistent with the enhancing effect of cusp precipitation on preexisting EUV-generated plasma [*Rodger et al.*, 1994]. During their transpolar evolution, the patches decreased their density and twisted, changing their shape. When they reached the nightside auroral oval, the patches were dragged into a "T" shape as they exited the polar cap [*Robinson et al.*, 1985], confirming that the patches could only leave the polar cap at locations that mapped to ongoing magnetotail reconnection [*Zhang et al.*, 2013b; *Foster et al.*, 2014; *Lorentzen et al.*, 2004;

Table 1. The Time of the Polar Cap Entry and Exit and Completely Fading of Each Patch, Together With Its Cross-Cap Transit Time and Lifetime as Well as the Evolution Distance of the Magnetic Field Lines, Associated With the Front Edges of the Patches, From Their Open to Reclose Due to the Dayside and Nightside Reconnections

Patch No.	Entry (UT)	Exit (UT)	Disappear (UT)	Cross-Cap Transit Time (h)	Evolution Distance(Re)	Lifetime (h)
P1	18:15	20:20	21:40	~2.1	450	~3.4
P2a	19:25	20:25	20:55	1.0	215	1.5
P2b	19:25	20:35	21:25	~1.2	258	2.0
P2c	19:25	20:35	22:25	~1.2	258	3.0
P3	19:20	21:05	21:25	~1.8	387	~2.1
P4a	19:45	20:55	21:05	~1.2	258	~1.3
P4b	19:45	21:20	21:30	~1.6	344	~1.8
P4c	19:45	21:45	22:55	2.0	429	~3.2
P5a	20:15	21:35	21:55	~1.3	279	~1.7
P5b	20:15	22:05	23:05	~1.8	387	~2.8
P5c	20:15	22:15	23:40	2.0	429	~3.4

Moen et al., 2007]. After exiting the polar cap, the patches evolved into "blobs" in the auroral sunward return flow region on the duskside and/or dawnside (see Figures 2e–2i). The full evolution of these patches can be seen most clearly in Movie S1 in the supporting information, which is the 5 min resolution movie of the same data set as shown in Figure 2.

In order to track each patch in some detail, we have picked a point on the leading edge of each patch and extracted the TEC value at that point from each TEC map. Figure 3 presents the time series evolution of the TEC (after median filtering by 3 × 3 points around the selected point in each TEC map), together with the trajectories of the selected points. Although these points have been selected by eye, which may result in some artificial effects on the trajectories and their associated TEC, they clearly define the patch evolution. We define the entry of the patch into the polar cap as the point where the TEC rises under the influence of the cusp precipitation and define the exit as the point where the trajectory turns from antisunward to east/west/sunward and the TEC decreases. We mark these entries and exits by vertical red dashed lines. From Figure 3, we can see that the TEC inside each patch increased as it entered the polar cap, maintained a relatively high value in the polar cap and quickly decayed to about 4–15 TECU around the time of its exit from the polar cap. There are three potential causes for this rapid decay in density: (1) the polar rain precipitation was shut off by magnetotail reconnection [*Y. Zhang et al.*, 2011], (2) faster convection caused an enhanced plasma loss rate [*Lockwood et al.*, 2000], and (3) the effect of long residence times away from production by either EUV radiation or auroral precipitation, which would reduce the density even if the decay rates were not enhanced. Of these (3) does not appear to apply, because Figure 3 shows that on leaving the polar cap, the slow antisunward migration of the patches turned to rapid eastward or westward motion. Notice that the TEC in some of the patches slightly increased after they exited the polar cap, which can be attributed to precipitation in the nightside auroral oval.

Figure 3 shows that the trajectory of patch P1 was directed toward the dawnside after it left the polar cap. This patch reached the dayside and completely faded in the morning sector sunward return flow. On the other hand, patch P3 moved only slightly duskward and completely faded near midnight. The other patches each divided into three parts, whose trajectories evolved either dawnward or duskward, possibly because the nightside reconnection occurred in different MLT sectors at different times [*Mishin et al.*, 2001; *Cheng et al.*, 2002; *Liu et al.*, 2010]. It is worth noting that patches P2a and P5a exited the polar cap around 19:00 MLT, which may suggest that the tail reconnection occurred at the dusk flank around this time. The cross-cap transit time and lifetime of each patch are shown in Table 1. The transit times of these patches may conceivably be somewhat less than the total transit times of the corresponding field lines, since it is possible that the field lines may have been opened (and hence their antisunward motion may already have started) before the first increase in total electron content occurred. Also, it is possible that the open-closed field line boundary might have been located equatorward of the terminator, in which case the patch might have been difficult to distinguish during the initial part of the field line transit, due to the high density of the background plasma. Recognizing that they may be slightly underestimated, the cross-cap transit times were in the range of 1.0–1.3 h for patches P2a, P2b, P2c, P4a, and P5a (see the fifth row of Table 1), which were potentially associated with tail reconnection occurring at the dusk flank, while the

transit times range between 1.6 and 2.1 h for the other patches or the other branches of patches (see the fifth row of Table 1), which may be associated with the tail reconnection in the midnight sector. These transit times are consistent with previous reports of 130 min flux transport time from the dayside magnetosphere to the magnetotail plasma sheet [*Pitkänen et al.*, 2013] but are much shorter than the time scales of 3–4 h inferred from the averaged interval between IMF B_y changes and the formation of transpolar arcs, reported by *Fear and Milan* [2012]. Using our measured transit times and the average solar wind velocity during this period (about 380 km/s), we can roughly deduce that the magnetic field lines threading the front edges of the patches must have evolved over distances of between 215 and 450 Re in the solar wind, from the time of their opening at the dayside magnetopause to their reclosure by nightside reconnection. It is worth noting that the total lifetimes for patches P1, P2c, P4c, and P5c, which evolved through almost a full Dungey cycle from dayside to nightside and back to dayside from the dawn flank, ranged from about 3.0 to 3.4 h, while the lifetimes of the other patches or the weaker branches of patches (see the seventh row of Table 1) were in the range from about 1.5 to 2.8 h. This suggests that the time taken for the full circulation of energy and momentum from the solar wind to the magnetosphere was about 3 h. The variety of the transit times and trajectories shown in Table 1 and Figure 3 emphasizes the variability in patch evolution due to the nonsteady nature of both magnetopause and tail reconnection and the consequent variations in convection which they generate.

### 2.3. Tromsø Magnetometer and EISCAT Tromsø UHF Radar Observations

Tromsø (in northern Norway) was located near the nightside polar cap boundary during the interval of interest (shown as the mauve star with "TRO" in each panel of Figure 2) and was therefore an ideal place to monitor the local signature of ongoing magnetotail reconnection and the exit of patches from the polar cap. It is well known that auroral substorm intensifications are associated with negative deflections in the H component of the ground magnetometer [e.g., *Lorentzen et al.*, 2004]. Such negative deflections are a ground signature of the diverted tail current closing in the ionosphere via the westward electrojet and are indicative of an enhanced reconnection rate [cf. *Russell and McPherron*, 1973; *Lorentzen et al.*, 2004]. The H component of the magnetic field measured by the magnetometer at Tromsø is shown in Figure 4a. The EISCAT Tromsø UHF radar was also operated after 20:45 UT on this day and was pointing close to the field-aligned direction (azimuth −173.8°, elevation 77.5°). The EISCAT data covered the altitude range from about 80 to 670 km. The bottom five panels in Figure 4 present 2 min postintegrations of the UHF radar observations between 20:45 and 22:45 UT (about 23:15 to 01:15 magnetic local time (MLT)) on 17 January 2013. Parameters shown are (b) electron density, (c) electron temperature, (d) ion temperature, (e) line of sight ion velocity, and (f) the integrated total electron content along the radar beam (up to 670 km altitude) and the averaged GPS TEC at Tromsø, as a function of altitude and time.

From Figure 4, we can see that there were six negative deflections, marked by S1-6, in the H component (Figure 4a), which we associate with six intervals of ongoing magnetotail reconnection. During each negative deflection, there were clear electron precipitation events, reaching down to about 100 km and enhancing the electron temperature in the F region and the electron concentration in the E region (Figures 4c and 4b, respectively). These ionospheric signatures are consistent with intermittent local magnetotail reconnection [*Wood et al.*, 2009], while the ion temperature and ion line of sight velocity showed evidence of slight heating and upwelling (Figures 4d and 4e), associated with Joule heating. Even though the Tromsø magnetogram sometimes suggests an apparent overlap between the magnetometer deflections and the occurrence of the patches (e.g., in the case of events S3 and P4c), the EISCAT data make clear that the patches are generally well separated from the precipitation events and their associated electron temperature enhancements, the only exception being for patch P5b, when the magnetometer deflection (S5) is in any case rather small. Outside the magnetically disturbed intervals, particularly at the beginning of the interval shown in Figure 4, the electron density was well structured in the F region, showing clear enhancements reaching about 4×10^{11} cm^{-3}, while the electron temperature decreased and the ion temperature was slightly enhanced within these density enhancements (Figures 4b–4d). These density enhancements are characteristic of well-defined polar cap patches, consistent with previous observations of high electron density and low electron temperature within the patches reported by *Moen et al.* [2004] and *Q.-H. Zhang et al.* [2011, 2013a]. These data show that the patches were simply transported through the polar cap by the transpolar plasma flow. We have highlighted these patches by two dashed black vertical lines and marked by P2b, P4a-c, and P5b-c for comparison with the branches of the patches
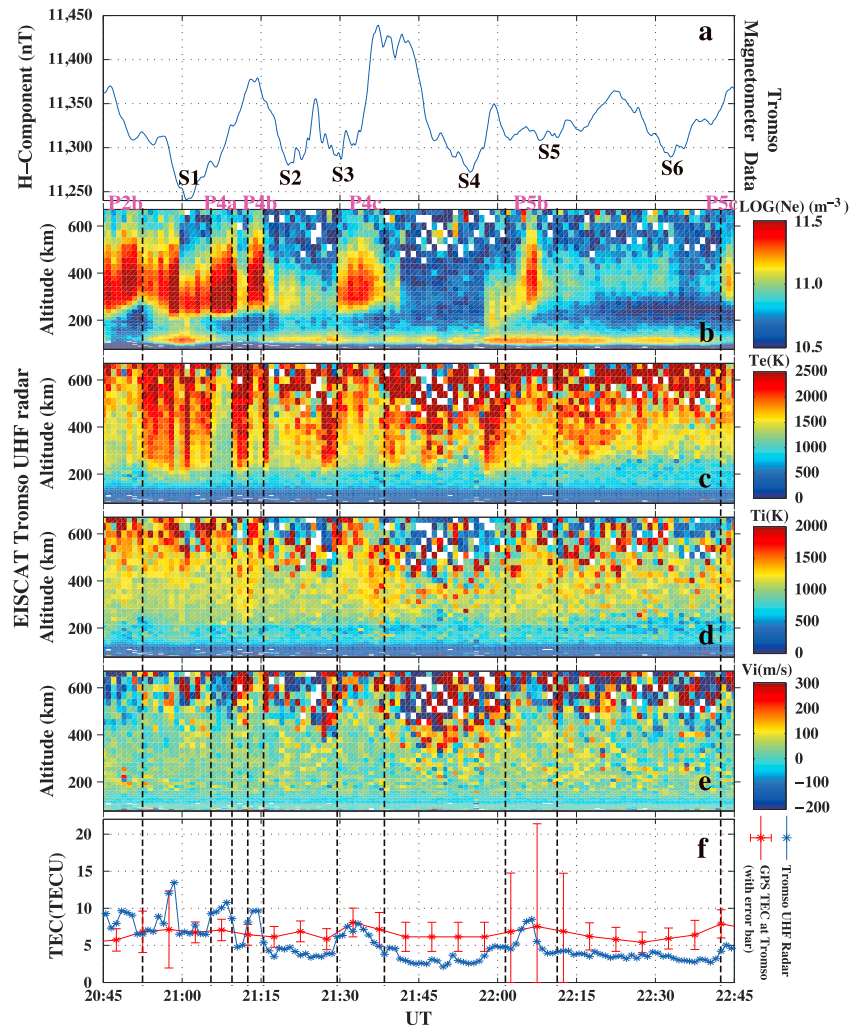
Figure 4. The magnetic field observed by the Tromsø magnetometer and plasma parameters observed by EISCAT Tromsø UHF radar between 20:45 and 22:45 UT on 17 January 2013. Data are (a) the horizontal component of the magnetic field; (b) Ne, electron density; (c) Te, electron temperature; (d) Ti, ion temperature; (e) Vi, the line-of-sight velocity (positive away from the radar); and (f) the averaged GPS TEC and integrated UHF radar TEC as a function of time and altitude.

shown in Figures 2 and 3. The separation between the patches and the periods of electron precipitation (with the exception of the period of the small deflection S5) suggests that the nightside PCB moved equatorward, associated with electron precipitation due to the magnetic field reclosure associated with the nightside reconnection, enabling the patches to exit the polar cap in the interval immediately following the electron precipitation events. This strongly supports the concept that the patches could only exit the polar cap at locations that mapped to ongoing magnetotail reconnection [*Zhang et al.*, 2013b; *Lorentzen et al.*, 2004]. The integrated TEC enhancements shown in the EISCAT UHF radar data matched well to the arrival times of patches seen in the GPS TEC data at Tromsø (Figure 4f) The radar integrated TEC, however, is much larger than the GPS TEC, and the patches seen in the radar data correspond more to an increase in the GPS TEC uncertainty rather than its mean value. This is partly because the time resolution of the radar TEC data is 2 min and hence shorter than the GPS TEC data, which means that small-scale structure in the *F* region plasma passing through the beam is measured by the radar but not resolved in the GPS measurements. In addition, the GPS data would be averaged across these small-scale structures, due to the fact that the oblique propagation of the signal between the individual receiver-satellite pairs used in making the measurement implies a range of *F* region penetration locations and elevation angles for the propagation path. Furthermore, the inversion to produce vertical TEC from the GPS slant-range observation assumes a "regular" *F* region profile (e.g., Chapman layer). Differences from this model ionosphere will create further
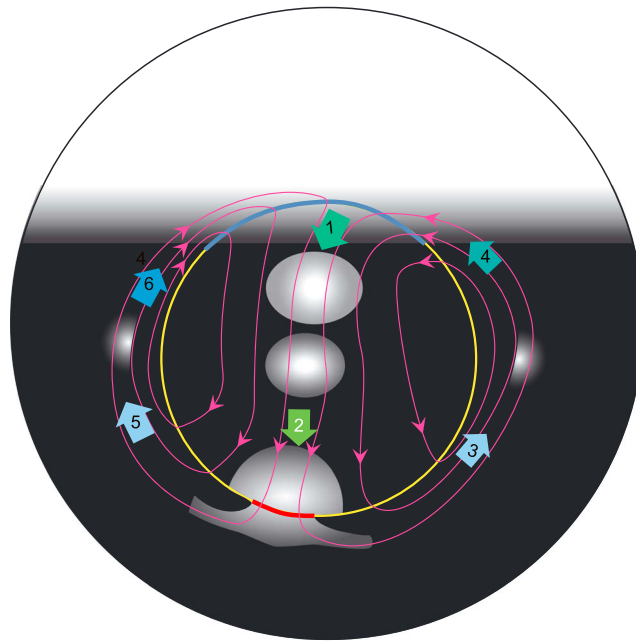
Figure 5. Schematic of the northern polar ionosphere during a substorm growth phase with southward IMF and $B_y < 0$. Convection streamlines are in mauve. The boundary between open and closed field lines (OCB) lies close to the poleward edge of the auroral oval: the blue/red OCB segments show where magnetic reconnection at the magnetopause/magnetotail is generating/destroying open flux in the Dungey convection cycle. In this case, magnetopause reconnection is dominant and the polar cap is expanding. The yellow OCB segments are adiaroic (meaning "not flowing across") though flow streamlines cross the OCB because it is in motion and the plasma moves with it. The grey scale indicates plasma concentration, with white showing high values generated by solar EUV and black showing low values where plasma has decayed on the nightside. Convection leads to high-density plasma entering the polar cap from subauroral latitudes (arrow 1). The patches are then transported antisunward across the polar cap (arrow 2) and evolve into blobs. These have been seen leaving the polar cap on the nightside but can only do so at locations that map to ongoing magnetotail reconnection. This intermittent exit produces the plasma blobs seen in the auroral sunward return flow region on the dusk (arrows 5 and 6) and/or dawn side (arrows 3 and 4).

differences in the comparison with the signal from a narrow-beam incoherent scatter radar. Also, note that some of the patches seen in the radar data appear more significant because, while their total electron content is similar to other patches, the density is concentrated over a narrower altitude range. Such effects can arise, for example, due to variations in temperature, which affect the plasma scale height. Figure 4f therefore suggests that patch signatures identified using a time series of densities around the *F* region peak might appear much more clear-cut than the corresponding signatures in TEC data.

3. Discussion and Conclusions

In Figure 2 the patches were seen being formed around the cusp region, due to the expansion and contraction of the polar cap boundary associated with the pulsed dayside magnetopause reconnection [*Lockwood and Carlson*, 1992; *Q.-H. Zhang et al.*, 2011, 2013a]. Figures 2 and 3, however, clearly show that they grew in amplitude on passing through the cleft and then cusp region, indicating that they were enhanced by magnetosheath-like precipitation [*Rodger et al.*, 1994]. The reconnection was directly confirmed by the in situ observations

of accelerated flows by the THEMIS spacecraft at the magnetopause [*Walsh et al.*, 2014]. *Walsh et al.* [2014] coordinated the ionospheric (global GPS TEC) and magnetopause (THEMIS in situ measurements) observations during the same period and found that the spacecraft measurements showed signatures of intermittent or bursty reconnection at the magnetopause, corresponding to the occurrence of patches of enhanced TEC, convecting tailward on open field lines over the pole in the ionosphere. These authors noted the existence of the patches in passing, but did not make any attempt to investigate them in detail. After their formation, we have seen that the patches grew in size at different rates due both to precipitation and the variation in local convection velocities [*Q.-H. Zhang et al.*, 2011, 2013b] and were transported poleward, along trajectories which reflected the changing balance between dayside and nightside reconnection and their consequent effects on the convection pattern.

The patches were seen exiting the nightside auroral oval, breaking up into a number of plasma blobs, and returning sunward in the auroral return flow of the dawn and/or dusk convection cell, consistent with the predictions from the previous theories, observations, and trajectory analysis techniques [*Robinson et al.*, 1985; *Sojka et al.*, 1993; *Zhang et al.*, 2013b; *Crowley et al.*, 2000]. *Moen et al.* [2007] provided statistics showing that patches exit the polar cap from ~18:30–05:30 MLT with most exiting within a 3–4 h region centered on 23:30 MLT. In order for a patch to exit the polar cap, however, ongoing nightside

reconnection is required. Without this, the polar cap boundary is "adiaroic" (see Figure 5) and the patch can only migrate slowly equatorward with the expanding polar cap boundary (see in Figures 2d–2h and Figure 4) and so would remain in the nightside polar cap (as for the portion of the patch on the dawn convection cell in the schematic given in Figure 5). Such patches, trapped by a lack of tail reconnection, would decay as the only source of production would be any residual polar rain precipitation. This concept is confirmed by the observations from the local magnetometer and EISCAT UHF radar. Note that there was no new patch formation, nor a TOI in the polar cap (i.e., the TEC levels in the polar cap remained at relatively low levels, giving dark blue shading in Figure 2) after about 22:30 UT. This may be because either (1) the polar cap boundary (see also the HMB) contracted poleward due to the decrease in IMF B_z and/or the growth of Region 2 current shielding of the electric field; or (2) there was a lack of high-density sunlit plasma at the right place for forming a TOI or patches, due to the low-density cavity rotating toward the afternoon sector; or (3) the dayside reconnection stopped at the associated magnetopause.

In Figure 5, we show an idealized view of the full evolution of these density features, demonstrating how the plasma patches are convected across the polar cap toward the nightside auroral oval, where the intermittent nature of tail reconnection restricts their ability to exit the polar cap and interacts with convection to decompose them into smaller plasma blobs, which then enter the return flow at auroral latitudes. It is important to emphasize, however, that such an idealized convection does not exist in practice; rather, the pattern is continuously evolving due to changing solar wind conditions and the balance between dayside and nightside reconnection rates. These changes determine which trajectories the patches and blobs actually follow. The advantage of the broad coverage of the GPS data used here is that they have enabled us to track these trajectories as conditions changed.

The patches were initially segmented from the SED at the equatorward edge of the cusp by the expansion and contraction of PCB, due to the pulsed dayside magnetopause reconnection. After formation, the patches entered the polar cap and evolved in a transpolar direction. When they arrived at the nightside auroral oval, their exit from the polar cap was modulated by the pulsed ongoing nightside reconnection implicit in the substorm cycle of the magnetosphere. Their behavior thus depended very strongly on the time and location of their arrival near to the nightside polar cap boundary and the time and location of reconnection in the cross-tail current sheet. After exiting the polar cap, the patches broke up into a number of plasma blobs and evolved further in the sunward return flow of the dawn and/or dusk convection cell. The lifetimes of the patches which exhibited this full evolution suggest that the total duration of energy and momentum circulation from the solar wind to the magnetosphere was about 3 h.

References

Bythrow, P. F., Potemra, T. A. and Zanetti, L. J. (1984) Variation of the auroral Birkeland current pattern associated with the north–south component of the IMF, in *Magnetospheric Currents*, edited by T. A. Potemra, AGU, Washington, D. C., doi:10.1029/GM028p0131.
Chappell, C. R. (1974), Detached plasma regions in the magnetosphere, *J. Geophys. Res.*, *79*(13), 1861–1870, doi:10.1029/JA079i013p01861.
Cheng, C.-C., C. T. Russell, M. Connors, and P. J. Chi (2002), Relationship between multiple substorm onsets and the IMF: A case study, *J. Geophys. Res.*, *107*(A10), 1289, doi:10.1029/2001JA007553.
Chisham, G., et al. (2007), A decade of the Super Dual Auroral Radar Network (SuperDARN): Scientific achievements, new techniques and future directions, *Surv. Geophys.*, *28*, 33–109, doi:10.1007/s10712-007-9017-8.
Coster, A. J., J. Foster, and P. Erickson (2003), Monitoring the ionosphere with GPS: Space weather, *GPS World*, *14*(5), 42.
Cowley, S. W. H., and M. Lockwood (1992), Excitation and decay of solar wind-driven flows in the magnetosphere-ionosphere system, *Ann. Geophys.*, *10*, 103–115.
Crowley, G. (1996), Critical review of ionospheric patches and blobs, in *Review of Radio Science 1992–1996*, edited by W. R. Stone, pp. 619–648, Oxford Univ. Press, U. K.
Crowley, G., A. J. Ridley, D. Deist, S. Wing, D. J. Knipp, B. A. Emery, J. Foster, R. Heelis, M. Hairston, and B. W. Reinisch (2000), Transformation of high-latitude ionospheric F region patches into blobs during the March 21, 1990, storm, *J. Geophys. Res.*, *105*, 5215–5230, doi:10.1029/1999JA900357.
Dungey, J. W. (1961), Interplanetary magnetic field and the auroral zones, *Phys. Rev. Lett.*, *6*, 47–48.
Dunlop, M. W., et al. (2011), Extended magnetic reconnection across the dayside magnetopause, *Phys. Rev. Lett.*, *107*(2), 025004, doi:10.1103/PhysRevLett.107.025004.
Fear, R. C., and S. E. Milan (2012), The IMF dependence of the local time of transpolar arcs: Implications for formation mechanism, *J. Geophys. Res.*, *117*, A03213, doi:10.1029/2011JA017209.
Foster, J. C., and W. J. Burke (2002), SAPS: A new categorization for sub-auroral electric fields, *Eos Trans. AGU*, *83*(36), 393–394, doi:10.1029/2002EO000289.
Foster, J. C., and J. R. Doupnik (1984), Plasma convection in the vicinity of the dayside cleft, *J. Geophys. Res.*, *89*, 9107–9113, doi:10.1029/JA089iA10p09107.

Foster, J. C., A. J. Coster, P. J. Erickson, F. J. Rich, and B. R. Sandel (2004), Stormtime observations of the flux of plasmaspheric ions to the dayside cusp/magnetopause, *Geophys. Res. Lett.*, *31*, L08809, doi:10.1029/2004GL020082.

Foster, J. C., et al. (2005), Multiradar observations of the polar tongue of ionization, *J. Geophys. Res.*, *110*, A09S31, doi:10.1029/2004JA010928.

Foster, J. C., et al. (2014), Prompt energization of relativistic and highly relativistic electrons during a substorm interval: Van Allen Probes observations, *Geophys. Res. Lett.*, *41*, 20–25, doi:10.1002/2013GL058438.

Goldstein, J., B. R. Sandel, W. T. Forrester, and P. H. Reiff (2003), IMF-driven plasmasphere erosion of 10 July 2000, *Geophys. Res. Lett.*, *30*(3), 1146, doi:10.1029/2002GL016478.

Heppner, J. P., and N. C. Maynard (1987), Empirical high-latitude electric field models, *J. Geophys. Res.*, *92*(A5), 4467–4489, doi:10.1029/JA092iA05p04467.

Hones, E. W., Jr., and K. Schindler (1979), Magnetotail plasma flow during substorms: A survey with Imp 6 and Imp 8 satellites, *J. Geophys. Res.*, *84*(A12), 7155–7169, doi:10.1029/JA084iA12p07155.

Iijima, T., and T. A. Potemra (1978), Large-scale characteristics of field-aligned currents associated with substorms, *J. Geophys. Res.*, *83*(A2), 599–615, doi:10.1029/JA083iA02p00599.

Imber, S. M., S. E. Milan, and M. Lester (2013), The SuperDARN Heppner-Maynard Boundary as a proxy for the latitude of the auroral oval, *J. Geophys. Res. Space Physics*, *118*, 1–13, doi:10.1029/2012JA018222.

Kelley, M. C., B. G. Fejer, and C. A. Gonzales (1979), An explanation for anomalous ionospheric electric fields associated with a northward turning of the interplanetary magnetic field, *Geophys. Res. Lett.*, *6*, 301–304, doi:10.1029/GL006i004p00301.

King, J. H., and N. E. Papitashvili (2005), Solar wind spatial scales in and comparisons of hourly Wind and ACE plasma and magnetic field data, *J. Geophys. Res.*, *110*, A02209, doi:10.1029/2004JA010804.

Knudsen, W. C. (1974), Magnetospheric convection and the high-latitude F2 ionosphere, *J. Geophys. Res.*, *79*, 1046–1055, doi:10.1029/JA079i007p01046.

Liu, J.-M., B.-C. Zhang, Y. Kamide, Z.-S. Wu, Z.-J. Hu, and H.-G. Yang (2010), Observation of a double-onset substorm during northward interplanetary magnetic field, *J. Atmos. Sol. Terr. Phys.*, *72*(11–12), 864–868, doi:10.1016/j.jastp.2010.04.010.

Lockwood, M. (1993), Modelling the high-latitude ionosphere for time-varying plasma convection, *Proc. Inst. Elec. Eng. - H*, *140*, 91–100, doi:10.1049/ip-h-2.1993.0015.

Lockwood, M. (1997), The relationship of dayside auroral precipitations to the open-closed separatrix and the pattern of convective flow, *J. Geophys. Res.*, *102*(A8), 17,475–17,487, doi:10.1029/97JA01100.

Lockwood, M., and H. C. Carlson (1992), Production of polar cap electron density patches by transient magnetopause reconnection, *Geophys. Res. Lett.*, *19*(17), 1731–1734, doi:10.1029/92GL01993.

Lockwood, M., I. W. McCrea, S. E. Milan, J. Moen, J. C. Cerisier, and A. Thorolfsson (2000), Plasma structure within poleward-moving cusp/cleft auroral transients: EISCAT Svalbard radar observations and an explanation in terms of large local time extent of events, *Ann. Geophys.*, *18*, 1027–1042, doi:10.1007/s00585-000-1027-5.

Lockwood, M., J. A. Davies, J. Moen, A. P. van Eyken, K. Oksavik, I. W. McCrea, and M. Lester (2005), Motion of the dayside polar cap boundary during substorm cycles: II. Generation of poleward-moving events and polar cap patches by pulses in the magnetopause reconnection rate, *Ann. Geophys.*, *23*, 3513–3532.

Lorentzen, D. A., N. Shumilov, and J. Moen (2004), Drifting airglow patches in relation to tail reconnection, *Geophys. Res. Lett.*, *31*, L02806, doi:10.1029/2003GL017785.

McPherron, R. L., C. T. Russell, and M. P. Aubry (1973), Satellite studies of magnetospheric substorms on August 15, 1968: 9. Phenomenological model for substorms, *J. Geophys. Res.*, *78*(16), 3131–3149, doi:10.1029/JA078i016p03131.

Milan, S. E., G. Provan, and B. Hubert (2007), Magnetic flux transport in the Dungey cycle: A survey of dayside and nightside reconnection rates, *J. Geophys. Res.*, *112*, A01209, doi:10.1029/2006JA011642.

Mishin, V. M., T. Saifudinova, A. Bazarzhapov, C. T. Russell, W. Baumjohann, B. Nakamura, and M. Kubyshkina (2001), Two distinct substorm onsets, *J. Geophys. Res.*, *106*(13), 13,105–13,118, doi:10.1029/2000JA900152.

Moen, J., M. Lockwood, K. Oksavik, H. C. Carlson, W. F. Denig, A. P. van Eyken, and I. W. McCrea (2004), The dynamics and relationships of precipitation, temperature and convection boundaries in the dayside auroral ionosphere, *Ann. Geophys.*, *22*, 1973–1987.

Moen, J., N. Gulbrandsen, D. A. Lorentzen, and H. C. Carlson (2007), On the MLT distribution of F region polar cap patches at night, *Geophys. Res. Lett.*, *34*, L14113, doi:10.1029/2007GL029632.

Oksavik, K., V. Barth, J. Moen, and M. Lester (2010), On the entry and transit of high-density plasma across the polar cap, *J. Geophys. Res.*, *115*, A12308, doi:10.1029/2010JA015817.

Pitkänen, T., M. Hamrin, P. Norqvist, T. Karlsson, and H. Nilsson (2013), IMF dependence of the azimuthal direction of earthward magnetotail fast flows, *Geophys. Res. Lett.*, *40*, 5598–5604, doi:10.1002/2013GL058136.

Robinson, R. M., R. T. Tsunoda, J. F. Vickrey, and L. Guerin (1985), Sources of F region ionization enhancements in the nighttime auroral zone, *J. Geophys. Res.*, *90*(A8), 7533–7546, doi:10.1029/JA090iA08p07533.

Rodger, A. S., M. Pinnock, J. R. Dudeney, K. B. Baker, and R. A. Greenwald (1994), A new mechanism for polar patch formation, *J. Geophys. Res.*, *99*(A4), 6425–6436, doi:10.1029/93JA01501.

Ruohoniemi, J. M., and K. Baker (1998), Large-scale imaging of high-latitude convection with SuperDARN HF radar observations, *J. Geophys. Res.*, *103*(A9), 20,797–20,811.

Russell, C. T., and R. L. McPherron (1973), The magnetotail and sub- storms, *Space Sci. Rev.*, *15*, 205.

Shepherd, S. G., and J. M. Ruohoniemi (2000), Electrostatic potential patterns in the high latitude ionosphere constrained by SuperDARN measurements, *J. Geophys. Res.*, *105*(A10), 23,005–23,014, doi:10.1029/2000JA000171.

Siscoe, G. L. (1982), Energy coupling between regions 1 and 2 Birkeland current systems, *J. Geophys. Res.*, *87*(A7), 5124–5130, doi:10.1029/JA087iA07p05124.

Siscoe, G. L., and T. S. Huang (1985), Polar cap inflation and deflation, *J. Geophys. Res.*, *90*(A1), 543–547, doi:10.1029/JA090iA01p00543.

Sojka, J. J., M. D. Bowline, R. W. Schunk, D. T. Decker, C. E. Valladares, R. Sheehan, D. N. Anderson, and R. A. Heelis (1993), Modeling polar cap F-region patches using time varying convection, *Geophys. Res. Lett.*, *20*(17), 1783–1786, doi:10.1029/93GL01347.

Thomas, E. G., J. B. H. Baker, J. M. Ruohoniemi, L. B. N. Clausen, A. J. Coster, J. C. Foster, and P. J. Erickson (2013), Direct observations of the role of convection electric field in the formation of a polar tongue of ionization from storm enhanced density, *J. Geophys. Res. Space Physics*, *118*, 1180–1189, doi:10.1002/jgra.50116.

Walsh, B. M., J. C. Foster, P. J. Erickson, and D. G. Sibeck (2014), Simultaneous ground- and space-based observations of the plasmaspheric plume and reconnection, *Science*, *343*, 1122–1125, doi:10.1126/science.1247212.

Wood, A. G., S. E. Pryse, and J. Moen (2009), Modulation of nightside polar patches by substorm activity, *Ann. Geophys.*, *27*, 3923–3932.

Zhang, Q.-H., et al. (2011), On the importance of interplanetary magnetic field |By| on polar cap patch formation, *J. Geophys. Res.*, *116*, A05308, doi:10.1029/2010JA016287.

Zhang, Q.-H., et al. (2013a), Polar cap patch segmentation of the tongue of ionization in the morning convection cell, *Geophys. Res. Lett.*, *40*, 2918–2922, doi:10.1002/grl.50616.

Zhang, Q.-H., et al. (2013b), Direct observations of the evolution of polar cap ionization patches, *Science*, *339*, 1597–1600, doi:10.1123/science.1231487.

Zhang, Y., L. J. Paxton, and H. Kil (2011), Nightside polar rain aurora boundary gap and its applications for magnetotail reconnection, *J. Geophys. Res.*, *116*, A11214, doi:10.1029/2011JA016884.